Time-Dependent Density-Functional Description of the ^1L_a State in Polycyclic Aromatic Hydrocarbons: Charge-Transfer Character in Disguise?

Ryan M. Richard and John M. Herbert*

Department of Chemistry, The Ohio State University, Columbus, Ohio 43210, United States

Ⓢ *Supporting Information*

ABSTRACT: The electronic spectrum of alternant polycyclic aromatic hydrocarbons (PAHs) includes two singlet excited states that are often denoted ^1L_a and ^1L_b. Time-dependent density functional theory (TD-DFT) affords reasonable excitation energies for the ^1L_b state in such molecules, but often severely underestimates ^1L_a excitation energies and fails to reproduce observed trends in the ^1L_a excitation energy as a function of molecular size. Here, we examine the performance of long-range-corrected (LRC) density functionals for the ^1L_a and ^1L_b states of various PAHs. With an appropriate choice for the Coulomb attenuation parameter, we find that LRC functionals avoid the severe underestimation of the ^1L_a excitation energies that afflicts other TD-DFT approaches, while errors in the ^1L_b excitation energies are less sensitive to this parameter. This suggests that the ^1L_a states of certain PAHs exhibit some sort of charge-separated character, consistent with the description of this state within valence-bond theory, but such character proves difficult to identify a priori. We conclude that TD-DFT calculations in medium-size, conjugated organic molecules may involve significant but hard-to-detect errors. Comparison of LRC and non-LRC results is recommended as a qualitative diagnostic.

I. INTRODUCTION

Most contemporary density-functional approximations, including those based on generalized gradient approximations (GGAs) as well as hybrid functionals that do not incorporate full Hartree—Fock (HF) exchange, afford an incorrect asymptotic distance dependence for charge-transfer (CT) excitation energies.[1] In the context of time-dependent density functional theory (TD-DFT), this artifact leads to predictions of spurious, low-energy CT states in large molecules,[2–4] liquids,[5] and clusters.[6,7] One means to mitigate this problem, while retaining the computational simplicity of TD-DFT, is to use long-range-corrected (LRC) density functionals.[8–20] The basic idea behind LRC-DFT is to treat the electron—electron exchange interaction using HF theory at large separation, since HF theory affords the proper distance dependence for CT excitation energies,[1] but to use GGA exchange at short range, in the interest of obtaining an accurate description of dynamical electron correlation. This length-scale separation is accomplished by partitioning the electron—electron Coulomb operator into short- and long-range components.[8,15,21–23]

While conventional TD-DFT's propensity to overstabilize CT states[1–7] and Rydberg states[19,24] is well-known, this method's admirable accuracy for localized, valence excitations in small organic molecules is similarly well-documented.[25,26] For alternant polycyclic aromatic hydrocarbon (PAH) molecules, however, TD-DFT calculations sometimes afford large errors in excitation energies,[27,28] for states that one would not ordinarily associate with CT character.

A particular class of examples is the homologous sequence of linear-condensed acenes (benzene, naphthalene, anthracene, etc.), which exhibit two low-lying $^1\pi\pi^*$ excited states, commonly denoted ^1L_a and ^1L_b.[29–31] The transition densities for these two states are polarized along the short and long axes of the molecule, respectively (see Figure 1), with the ^1L_b transition density exhibiting nodes at the atoms and the ^1L_a transition density displaying nodes at the bond midpoints.[30,31] For the ^1L_a state in the linear acene sequence, errors in TD-DFT excitation energies increase dramatically as a function of the number of aromatic rings, yet errors in the ^1L_b excitation energies appear to be uncorrelated with molecular size.[27,32] (This is perhaps all the more surprising in view of the fact that the ^1L_b state in benzene and naphthalene exhibits substantial double-excitation character, whereas the ^1L_a state does not.[33–35]) Recently, however, certain TD-LRC-DFT have been shown to afford accurate ^1L_a excitation energies for the linear acenes, eliminating the length-dependent trend in the errors.[36,37]

The ^1L_a and ^1L_b states in linear acenes have long been discussed as being "ionic" and "covalent", respectively, in the language of valence-bond (VB) theory.[31] In other words, the ^1L_a wave function is thought to include determinants where both π electrons from a C=C bond are assigned to the same carbon atom. Detailed VB calculations corroborate this conceptual picture,[33–35,38] and this might lead one to suspect that charge separation in the ^1L_a state, which somehow increases as a function of molecular size, could explain the errors observed in TD-DFT excitation energies for the ^1L_a state. This is precisely what was concluded in a recent study,[27] based on a semiempirical charge-decomposition analysis. The goal of the present work is to analyze all-electron TD-DFT and TD-LRC-DFT calculations of ^1L_a and ^1L_b on a more diverse set of PAHs.
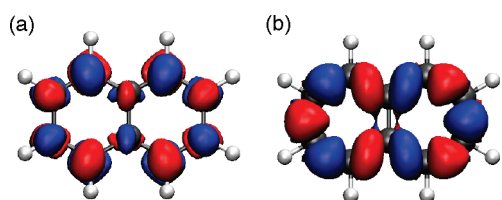
Figure 1. Transition densities for (a) the ^1L_a state and (b) the ^1L_b state of naphthalene, computed at the TD-B3LYP level. The isosurface in either plot encapsulates 90% of the transition density.

II. METHODS

Ground-state geometries were optimized at the B3LYP/6-31G* level, and vertical excitation energies (for singlet states only) were subsequently calculated at the TD-DFT/cc-pVTZ level, using various density functionals. The SG-1 quadrature grid[39] was used for all TD-DFT calculations, as tests using significantly finer grids resulted in changes of less than 0.01 eV in the excitation energies. Except where noted, the commonly used Tamm−Dancoff approximation[40] is *not* employed here. All calculations were performed using a locally modified version of Q-Chem.[41] Cartesian coordinates for the optimized PAH geometries, along with tabulated TD-DFT excitation energies, can be found in the Supporting Information.

A variety of LRC density functionals are examined in this work, including LRC-μBLYP, LRC-μBOP, LRC-ωPBE, and LRC-ωPBEh. The notations "μBLYP" and "μBOP" indicate that the BLYP[42,43] and BOP[44] functionals are used, but with a short-range version of Becke's GGA exchange functional[42] that is constructed according to the prescription developed by Hirao and co-workers.[8] The notation "ωPBE" indicates a short-range version of the PBE exchange functional,[45] constructed according to the procedure of Scuseria and co-workers.[15] (The aforementioned notation is consistent with that used in the Q-Chem program but differs from the nomenclature used in some recent papers.[46]) The LRC-ωPBEh function is a hybrid ("h") that includes 20% HF exchange at short range.[19] All of the LRC functionals examined here include full HF exchange at long range:

$$E_{xc}^{LRC} = E_c + E_x^{GGA, SR} + C_{HF}E_x^{HF, SR} + E_x^{HF, LR} \qquad (1)$$

Here, "SR" and "LR" indicate use of the short-range and long-range components of the Coulomb operator, respectively, and C_{HF} is the coefficient of short-range HF exchange.
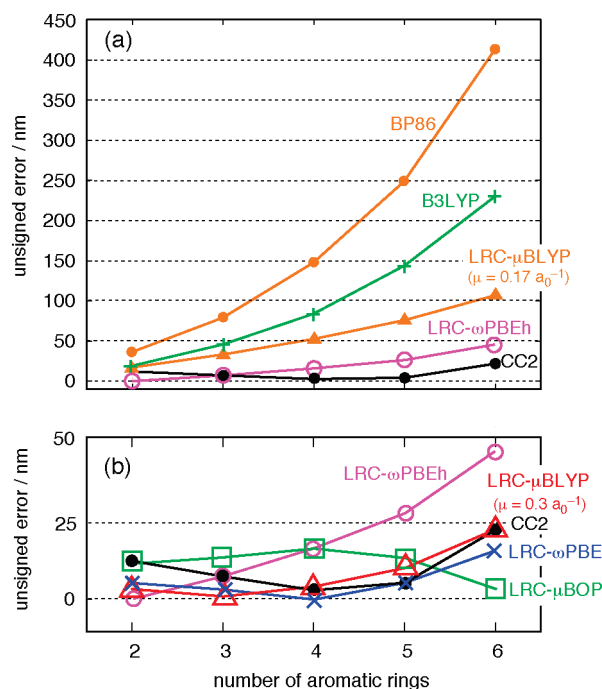
TD-LRC-DFT excitation energies can be quite sensitive to the value of the Coulomb attenuation parameter (μ or ω),[18,19] especially for CT-type excitations.[49] Values of μ or ω that are optimized using ground-state properties (e.g., atomization energies, ionization potentials, or reaction barrier heights) may afford large errors in TD-DFT excitation energies.[18,19] Previous studies by our group[4,19] have shown that LRC-ωPBE with ω = 0.3 a_0^{-1} and LRC-ωPBEh with ω = 0.2 a_0^{-1} afford the best statistical performance for excitation energies, without degrading ground-state properties. As such, we focus primarily on these two functionals. With the aforementioned parameters, the LRC-ωPBEh functional affords average errors of ~0.3 eV for both localized and CT excitation energies,[19] while the LRC-ωPBE functional performs similarly when ω lies in the range of 0.2−0.3 a_0^{-1}.[4,26]

As compared to LRC functionals based upon ωPBE, the functionals μBLYP and μBOP, which utilize the short-range

Table 1. Parameters for the LRC Functionals Employed in This Work

| functional	μ or ω/a_0^{-1}	C_{HF}	functional	μ or ω/a_0^{-1}	C_{HF}
LRC-μBOP	0.47	0.0	LRC-ωPBE	0.30	0.0
LRC-μBLYP[a]	0.17	0.0	LRC-ωPBEh	0.20	0.2
LRC-μBLYP[a]	0.30	0.0			

[a] Two different values of μ are used for LRC-μBLYP.

Figure 2. TD-DFT errors in the vertical excitation energies for the ^1L_a state, expressed in wavelength units. Panel (a) illustrates the divergence of the TD-B3LYP and TD-BP86 excitation energies as a function of n, while panel (b) shows a close-up view of the errors engendered by several different LRC functionals.

"μB88" functional[46] developed by Hirao and co-workers,[8] have not been studied as extensively in the context of TD-DFT excitation energies. It does appear that the LRC-μPBE and LRC-ωPBE functionals afford comparable excitation energies, at a given value of the Coulomb attenuation parameter (μ or ω),[19] although predicted ground-state properties may be quite different.[18]

In view of these facts, we choose the value μ = 0.3 a_0^{-1} for the LRC-ωPBE and LRC-μBLYP functionals, a choice that is supported by results from a recent TD-LRC-DFT study of linear acenes.[37] At the same time, the value μ = 0.17 a_0^{-1} was found to provide the most accurate excitation energies in a recent TD-LRC-μBLYP study of intramolecular CT states in Coumarin dyes,[50] although the value μ = 0.31 a_0^{-1} performs better for oligothiophenes.[51] Thus, for completeness we will consider LRC-μBLYP with μ = 0.17 a_0^{-1}. Finally, Hirao and co-workers advocate the use of LRC-μBOP with μ = 0.47 a_0^{-1},[10] so we will assess this functional as well, even though our previous work indicates that values of $\mu \gtrsim 0.5$ a_0^{-1} often afford large errors in ground-state properties.[18] Table 1 lists the parameters for each of the LRC functionals used in this work.
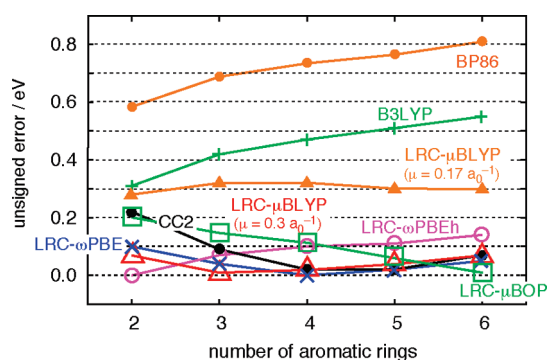
Figure 3. TD-DFT errors in the vertical excitation energies for the ^1L_a state of the linear acene sequence, expressed in energy units.

III. RESULTS

A. Linear-Condensed Acenes. The ^1L_a and ^1L_b states in the linear-condensed acene series are characterized by transition densities that are polarized along the short and long axes of the molecule, respectively,[30,31] as illustrated for naphthalene in Figure 1. Consistent with previous calculations,[27,33–35,37,38,52] we find that the $S_0 \rightarrow {}^1L_a$ excitation is dominated (>90%) by a transition between the highest occupied and lowest unoccupied molecular orbitals (HOMO → LUMO), whereas the $S_0 \rightarrow {}^1L_b$ excitation involves (HOMO − 1) → LUMO and HOMO → (LUMO + 1) transitions, with approximately equal weights.

As noted in previous studies,[27,32,37] errors in the ^1L_a excitation wavelength computed using TD-DFT methods often increase rapidly as a function of the number of aromatic rings, n. Errors in the ^1L_a excitation wavelength are plotted in Figure 2 as a function of n, for the set of functionals considered here. (We note that Wong and Hsieh[37] have recently published similar results, using a slightly different set of LRC functionals.) Also included in Figure 2 are the errors obtained using approximate coupled-cluster theory (CC2), which were obtained from ref 27. Errors are computed on the basis of experimental band maxima that have been corrected to account for excited-state geometry relaxation.[27]

Wong and Hsieh[37] have noted previously that size-dependent errors in the ^1L_a excitation wavelength that are obtained at the TD-BP86 and TD-B3LYP level are greatly reduced using certain TD-LRC-DFT approaches, for which a qualitatively correct distance dependence is obtained. Our results add a caveat, namely, that the erroneous n-dependence of the excitation wavelength remains in LRC-μBLYP calculations performed using $\mu = 0.17\ a_0^{-1}$. This value of μ, which was suggested in two different studies of CT states in Coumarin dyes,[50,53] is the smallest value of the Coulomb attenuation parameter that has been suggested in any benchmark study of LRC-DFT of which we are aware. Other LRC functionals examined here use a Coulomb attenuation parameter of either $0.2\ a_0^{-1}$ or $0.3\ a_0^{-1}$, and for these functionals the errors in ^1L_a excitation wavelengths for the linear acene series is uncorrelated with molecular size.

At the same time, one should recognize that the length-dependent trends that are evident in the excitation *wavelength* data in Figure 2 amount to relatively small changes in excitation *energies*, at least in comparison to the ∼0.3 eV statistical error bar that is typically ascribed to TD-DFT calculations. Errors in excitation energies for the ^1L_a state of the linear acene sequence are shown in Figure 3. From these data, it is difficult to ascribe any

Table 2. Mean Absolute Errors (MAEs) in Excitation Energies for the Linear Acene Sequence, $n = 2-6$

method	MAE ^{a}/eV	
	^1L_a	^1L_b
CC2^b	0.08	0.22
TD-BP86	0.72	0.62
TD-B3LYP	0.45	0.15
TD-LRC-μBLYP ($\mu = 0.17\ a_0^{-1}$)	0.30	0.18
TD-LRC-μBLYP ($\mu = 0.30\ a_0^{-1}$)	0.07	0.31
TD-LRC-ωPBE	0.04	0.33
TD-LRC-ωPBEh	0.08	0.35
TD-LRC-μBOP	0.08	0.37

^{a} Relative to experimental values corrected for excited-state geometry relaxation (from ref 27). ^{b} Values taken from ref 27.
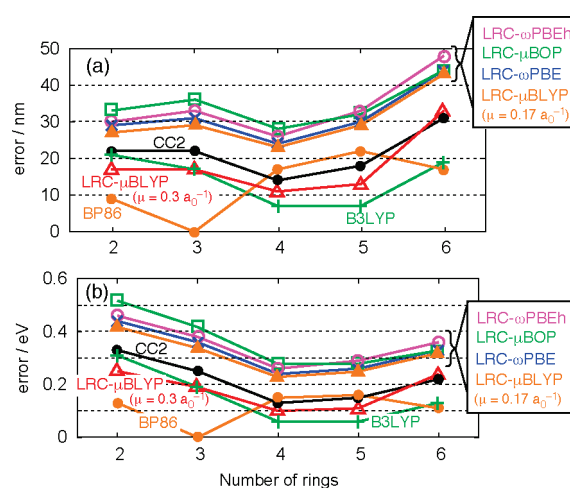
Figure 4. TD-DFT errors in the vertical excitation energies for the ^1L_b state, expressed in (a) wavelength units and (b) energy units.

length-dependent trend to the errors obtained using LRC-μBLYP($\mu = 0.17\ a_0^{-1}$); rather, these excitation energies appear to be systematically overestimated by about 0.3 eV. [Mean absolute errors (MAEs) for each method are listed in Table 2.] Excitation energies calculated using LRC-ωPBE ($\omega = 0.3\ a_0^{-1}$) and LRC-μBLYP ($\mu = 0.3\ a_0^{-1}$) are in good agreement with CC2 calculations. As noted by Wong and Hsieh,[37] LRC functionals significantly outperform B3LYP for the ^1L_a excitation energies, but B3LYP affords a smaller MAE for the ^1L_b excitation energies.

In contrast to the ^1L_a results, TD-DFT errors for the ^1L_b excitation energies show no clear trend with respect to n, even for the non-LRC functionals (see Figure 4). With the exception of the TD-BP86 calculations, the n-dependence of the TD-DFT errors tracks the CC2 results quite well, albeit with a constant energy offset that varies from one functional to another. This observation, along with the fact that the CC2 MAE is somewhat larger for ^1L_b than for ^1L_a (0.22 eV versus 0.08 eV), suggests that the correction applied to the experimental band maxima in order to obtain an experimental estimate of the vertical excitation energy[27] may be somewhat less accurate for ^1L_b. In any case, most of the TD-DFT MAEs for the ^1L_b state are $\lesssim 0.3$ eV, which is within the generally accepted accuracy of TD-DFT excitation energies.

Table 3. Comparison of Excitation Energies (in eV) for the ^1L_a State of the Linear Acene Sequence, Computed Using Full TD-DFT and also the Tamm−Dancoff Approximation (TDA)

	LRC-ωPBE		LRC-ωPBEh	
n	TD-DFT	TDA	TD-DFT	TDA
2	4.76	5.01	4.66	4.89
3	3.64	3.92	3.53	3.80
4	2.88	3.19	2.78	3.07
5	2.35	2.69	2.26	2.57
6	1.97	2.31	1.88	2.21

Another point worth noting is the effect of the Tamm−Dancoff approximation (TDA).[40] In benchmark calculations for small molecules, this approximation provides excitation energies within 0.15 eV of full TD-DFT results, at somewhat reduced cost. In larger molecules, however, we have observed that TD-DFT/TDA discrepancies are sometimes more significant. Table 3 summarizes the difference between TDA and full TD-DFT excitation energies for two different density functionals. We find that the TDA systematically increases both the ^1L_a and ^1L_b excitation energies, by about 0.3 eV. In the case of the ^1L_a state, a 0.3 eV shift would bring the TD-LRC-μBLYP ($\mu = 0.17\ a_0^{-1}$) excitation energies into good agreement with experiment, thereby masking errors that appear to indicate a too-small value of μ. In fact, it has previously been suggested that TD-DFT calculations on PAHs *should* invoke the TDA, as more accurate results are obtained (using B3LYP) with the TDA than with full TD-DFT.[52] In our view, this is most likely a fortuitous cancellation of errors, as only full TD-DFT affords the proper linear response of the ground-state density.

It has been determined, experimentally, that the ^1L_a state lies above the ^1L_b state for $n \leq 2$, but that ^1L_b is higher in energy starting at $n = 3$.[54] Both TD-B3LYP and TD-BP86 calculations incorrectly predict that ^1L_b is higher in energy starting at $n = 2$, whereas all of the TD-LRC-DFT methods examined here, with the exception of LRC-μBLYP with $\mu = 0.17\ a_0^{-1}$, place ^1L_a and ^1L_b in the correct energetic order as a function of molecular size, both within the TDA and also at the full TD-DFT level. The failure of TD-B3LYP in this context is potentially a problem in applications beyond PAHs, since indole (and, consequently, tryptophan) also exhibits ^1L_a and ^1L_b states, whose electronic structure is thought to be similar to the corresponding states in naphthalene.[55] TD-B3LYP also fails to predict the correct order of the ^1L_a and ^1L_b states in tryptophan.[56]

B. Nonlinear PAHs. Although LRC-DFT calculations of the linear acenes have been reported previously,[36,37] these methods have not yet been studied for more general, nonlinear PAHs. The TD-B3LYP and TD-BP86 methods *have* been applied to certain larger PAHs, and large errors in the ^1L_a excitation energies are observed in some cases.[28,52] Here, we apply TD-LRC-DFT to a set of nonlinear PAHs, the structures of which are depicted in Figure 5. This data set includes both cata-condensed and peri-condensed examples,[31] ranging in size from three to seven six-membered rings. A numbering scheme for these molecules is introduced in Figure 5; as a rough guideline, larger numbers correspond to larger molecules, although the data set does contain several structural isomers.

For these molecules, we shall restrict our calculations to the functionals B3LYP, LRC-ωPBE, and LRC-ωPBEh. Results
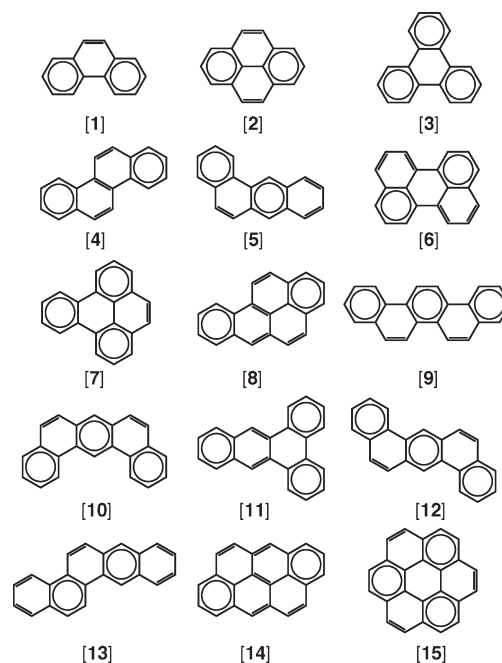

Figure 5. Clar-type resonance structures[57,58] of the nonlinear PAHs considered in this work, along with the numbering scheme that is used to refer to them in the text and figures: phenanthrene (**1**), pyrene (**2**), triphenylene (**3**), chrysene (**4**), benz[*a*]anthracene (**5**), perylene (**6**), benzo[*e*]pyrene (**7**), benzo[*a*]pyrene (**8**), picene (**9**), dibenz[*a,j*]anthracene (**10**), dibenz[*a,c*]anthracene (**11**), dibenz[*a,h*]anthracene (**12**), benzo[*b*]chrysene (**13**), anthanthrene (**14**), and coronene (**15**).
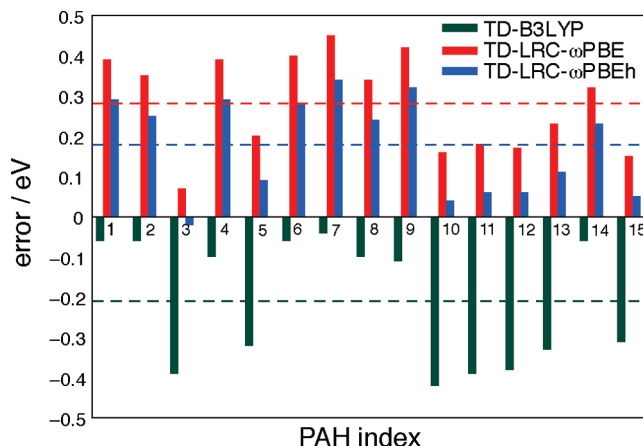
Figure 6. Errors (theory minus experiment) in ^1L_a excitation energies for the PAHs depicted in Figure 5. Dashed horizontal lines represent the average error for each method. Experimental benchmarks are band maxima in nonpolar solvents. The solvent correction suggested in ref 52 would reduce the TD-LRC-DFT errors by 0.11 eV and would make the TD-B3LYP errors more negative by 0.11 eV.

presented above and in ref 37 demonstrate that other LRC functionals afford very similar excitation energies for the linear acenes, provided that μ (or ω) is chosen appropriately. In particular, Wong and Hsieh[37] considered several different functionals with $C_{HF} = 0$ and $\mu \approx 0.3\ a_0^{-1}$ and found that MAEs across the linear acene sequence differ by no more than 0.05 eV, for both ^1L_a and ^1L_b. Our results (section III.A) show that μ can

1299

dx.doi.org/10.1021/ct100607w |*J. Chem. Theory Comput.* 2011, 7, 1296–1306
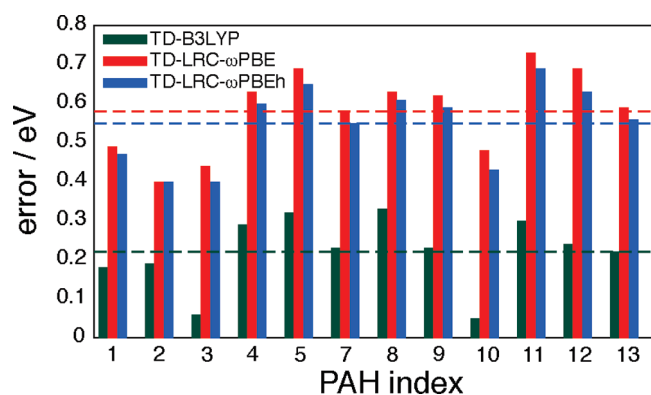
Figure 7. Errors (theory minus experiment) in ^1L_b excitation energies for the PAHs depicted in Figure 5. Dashed horizontal lines represent the average error for each method. Experimental benchmarks are band maxima in nonpolar solvents, and omissions from the data set in Figure 5 correspond to molecules for which no experimental value for the ^1L_b excitation energy is available. The solvent correction suggested in ref 52 would reduce all of the errors by 0.03 eV.

Table 4. Mean Absolute Errors (eV) in TD-DFT Excitation Energies for Various Subsets of Nonlinear PAHs

	MAE(^1L_a)[b]			MAE(^1L_b)[b]		
subset[a]	B3LYP	LRC-ωPBE	LRC-ωPBEh	B3LYP	LRC-ωPBE	LRC-ωPBEh
full set	0.32	0.17	0.07	0.19	0.55	0.52
cata	0.39	0.14	0.03	0.18	0.57	0.53
peri	0.22	0.23	0.12	0.22	0.51	0.49
1-2	0.36	0.17	0.06	0.19	0.57	0.53
3+	0.29	0.17	0.07	0.19	0.53	0.50

[a] The full data set is shown in Figure 5; see the text for a description of the various subsets. [b] Relative to solution-phase band maxima corrected for solvent effects.[52]

be reduced if short-range HF exchange is introduced, as in LRC-ωPBEh. This conclusion is in accord with previous findings using a more diverse set of molecules and excited states.[19]

Figure 6 shows the errors in the calculated vertical excitation energies for the ^1L_a state of the nonlinear PAHs. As in the case of the linear acenes, B3LYP consistently underestimates the excitation energies, with most of the largest errors associated with the larger PAHs. (Note that the errors in Figure 6 are signed quantities.) The two LRC functionals, on the other hand, consistently overestimate the excitation energies, which was also observed for the linear acene sequence, although the errors are somewhat larger here. Interestingly, the largest errors observed at the TD-B3LYP level seem to correlate with the smallest errors obtained using the LRC functionals.

We should note that the experimental excitation energies used to compute the TD-DFT errors are taken from ref 59 (they are also tabulated in ref 28) and represent band maxima in nonpolar solvents. On the basis of a comparison of solution-phase absorption spectra to gas-phase photoelectron spectra,[60] Wang and Wu[52] suggest that these values should be corrected upward by 0.11 eV to obtain an estimate of the gas-phase $S_0 \rightarrow {}^1L_a$ excitation energy. This correction has *not* been applied in Figure 6. If we were to apply this correction, then the mean error in ^1L_a excitation energies computed at the TD-B3LYP cc-pVTZ level would change from −0.21 eV (the value indicated in Figure 6) to −0.32 eV. Meanwhile, the TD-LRC-DFT values would become more accurate, with corrected mean errors of 0.1−0.2 eV, which is only slightly larger than the mean errors obtained for the linear acenes using these same LRC functionals.

Figure 7 depicts errors in the ^1L_b excitation energies for the nonlinear PAHs. (The solvent correction is also absent from these data, but the value suggested by Wang and Wu[52] is only 0.03 eV for the ^1L_b state.) As in the case of the linear acenes, all three of the TD-DFT methods consistently overestimate the ^1L_b excitation energies, with no clear size-dependent trend, and TD-B3LYP consistently outperforms the LRC functionals. For these molecules, the mean error in TD-LRC-DFT excitations energies (≈ 0.5 eV) is somewhat larger than for the ^1L_b states of the linear acenes and lies outside of the ∼0.3 eV accuracy established for these functionals in previous benchmark calculations.[4,19,26]

As mentioned above, for the nonlinear PAHs many of the largest TD-B3LYP errors for ^1L_a excitation energies coincide with the largest molecules in this data set, whereas TD-B3LYP errors tend to be smaller for the PAHs that are more condensed (in the sense of possessing more fused rings), and therefore smaller. To analyze this further, we have partitioned the full set of nonlinear PAHs into various subsets that reflect the degree and manner of annulation. In addition to cata-condensed and peri-condensed subsets, we consider a subset "1-2" in which each ring is fused to no more than two other rings, and another subset "3+" in which at least one ring is fused to three other rings.

Table 4 lists separate MAEs for each of these subsets, and these statistics do suggest that the accuracy of TD-B3LYP for the ^1L_a excitation energy is related to the extent of condensation. The cata-condensed and 1−2 subsets have MAEs that are larger than the MAE for the full data set, at the TD-B3LYP level, whereas in the case of the two LRC functionals, the MAE is largely unaffected by how the data set is partitioned. (For ^1L_b excitation energies, the MAE is largely unaffected by the partitioning even in the case of B3LYP.) However, this trend is not *strictly* related to molecular size. For example, the TD-B3LYP error for picene, **9**, is well below the mean, despite having one of the longer end-to-end distances among the nonlinear PAHs considered here.

IV. ANALYSIS AND DISCUSSION

A. Valence-Bond Considerations. One might hypothesize that size-dependent errors in ^1L_a excitation energies are related to well-known size-dependent errors in TD-DFT polarizabilities and hyperpolarizabilities for conjugated molecules,[61,62] problems that are mitigated when LRC functionals are employed.[63] Because the ^1L_b state exhibits no such size-dependent errors, however, we must look elsewhere for an explanation.

Grimme and Parac[27] have previously noted these size-dependent errors for the ^1L_a state and explained them in terms of an excited-state wave function having significant contributions from ionic determinants, to use valence-bond language. In other words, the valence-bond picture is that the ^1L_a wave function exhibits charge separation at the level of individual C−C bonds.[33−35] (The dipole moment of the ^1L_a state is zero, by symmetry, so the $S_0 \rightarrow {}^1L_a$ excitation cannot be associated with any *net* charge separation. In addition, the $S_0 \rightarrow {}^1L_a$ transition is primarily a HOMO → LUMO excitation, and both the HOMO and the LUMO are delocalized over the entire molecule, as required by symmetry.)

1300

dx.doi.org/10.1021/ct100607w |*J. Chem. Theory Comput.* 2011, 7, 1296–1306
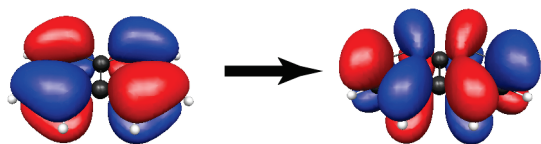
Figure 8. NTOs for the ^1L_a state of naphthalene, computed at the TD-B3LYP/cc-pVTZ level.
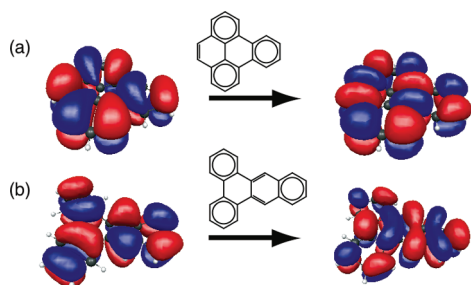

Figure 9. NTOs for two representative PAHs: (a) benzo[e]pyrene (**7**) and (b) dibenz[a,c]anthracene (**11**). The structure of each molecule is also shown. The NTOs shown in (a) accounts for 93% of the transition density, and those in (b) account for 84% of the transition density. Each NTO was computed at the TD-B3LYP/cc-pVTZ level.

Parac and Grimme[28] developed an "ionicity metric" based upon a Mulliken-style atomic partition of time-dependent Pariser—Parr—Pople[64−66] (TD-PPP) transition densities and demonstrated that this metric is strongly correlated with errors in excitation energies computed at the TD-BP86 level. We attempted a similar analysis, using transition densities computed from all-electron TD-DFT calculations, and taking proper account for the nonorthogonality of the atomic orbital (AO) basis. However, we found that the trends obtained from these all-electron calculations were far more muddled and ambiguous than those reported by Parac and Grimme, even when minimal basis sets were used in an effort to avoid well-known problems with Mulliken analysis in extended basis sets.

On the other hand, natural transition orbitals[67] (NTOs) for the ^1L_a state *do* support the notion of charge separation within the C−C bonds. As an example, Figure 8 depicts the most significant pair of NTOs for the ^1L_a state of naphthalene; this pair of NTOs accounts for 88% of the norm of the $S_0 \rightarrow {}^1L_a$ transition density matrix, and the product of these two NTOs is qualitatively similar to the $S_0 \rightarrow {}^1L_a$ transition density (cf. Figure 1a). The same sort of charge separation that is seen in this pair of NTOs might be inferred from the transition density itself, insofar as the latter has nodes centered on the C−C bonds, whereas the $S_0 \rightarrow {}^1L_b$ transition density has nodes located on the carbon atoms. These TD-B3LYP transition densities are consistent with the predictions of a simple particle-on-a-ring model,[30,31] which has long been used as a qualitative model for understanding the electronic structure of the linear acenes.

With the benefit of hindsight and the availability of VB calculations for naphthalene and anthracene,[33−35,38] this analysis of NTOs and transition densities for the linear acenes could be used to rationalize the size-dependence of TD-B3LYP results for the ^1L_a state and the lack of size dependence in TD-B3LYP results for the ^1L_b state. Analysis of the NTOs is more complicated in the case of the nonlinear PAHs, however. Consider two representative examples: benzo[e]pyrene (**7**), for which TD-B3LYP
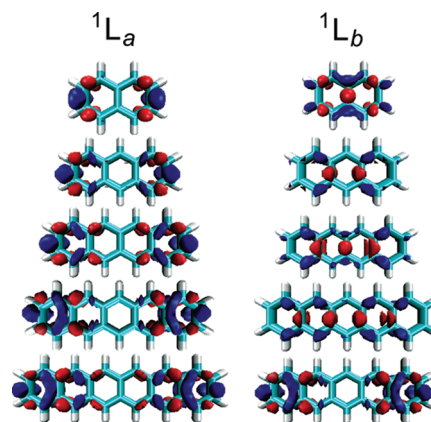
Figure 10. Difference densities, $\Delta\rho$, for the $S_0 \rightarrow {}^1L_a$ and $S_0 \rightarrow {}^1L_b$ excitations of the linear acene sequence, computed at the TD-B3LYP level. The two colored isosurfaces in each plot encapsulate 60% of the positive/negative part of $\Delta\rho$.
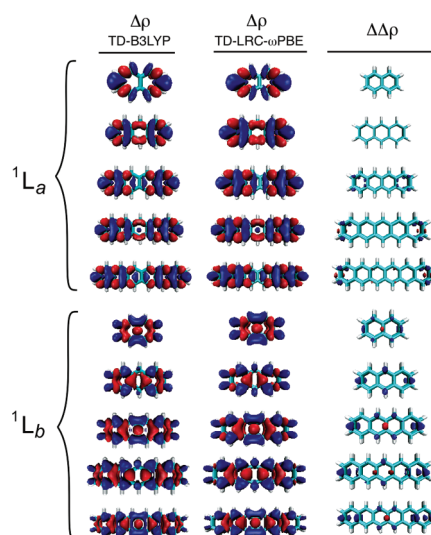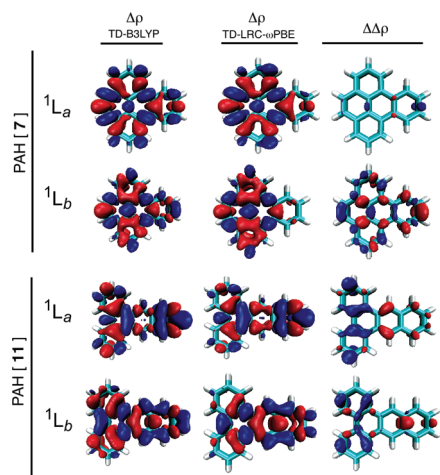

Figure 11. Difference densities, $\Delta\rho$, for the ^1L_a and ^1L_b states of the linear acene sequence computed using two different TD-DFT methods. The two colored isosurfaces in each plot encapsulate 95% of the positive negative part of $\Delta\rho$. The difference between the two difference densities, $\Delta\Delta\rho$, is also plotted, using the same isocontour that is used to plot $\Delta\rho$ at the TD-LRC-ωPBE level.

predicts an accurate ^1L_a excitation energy; and dibenz[a,c]-anthracene (**11**), for which TD-B3LYP significantly underestimates the ^1L_a excitation energy. The NTOs that dominate the $S_0 \rightarrow {}^1L_a$ transition for each of these two PAHs are pictured in Figure 9. In both cases, one could argue that the NTOs show evidence of charge separation within individual C−C bonds.

Detailed VB calculations are not generally available (or even feasible), and in their absence, we must conclude that one cannot unambiguously infer ionic character from NTOs and transition densities alone. Ideally, we would like a predictive means to diagnose errors in TD-DFT calculations. The search for such a diagnostic occupies the remainder of this work.

B. Difference Densities. To this end, we first examine difference densities,

$$\Delta\rho = \rho(\text{excited}) - \rho(\text{ground}) \tag{2}$$

Figure 12. Difference densities, $\Delta\rho$, for the ^1L_a and ^1L_b states of PAHs **7** and **11** computed using two different TD-DFT methods. The two colored isosurfaces in each plot encapsulate 95% of the positive negative part of $\Delta\rho$. The difference between the two difference densities, $\Delta\Delta\rho$, is also plotted, using the same isocontour as the TD-LRC-ωPBE plots.

for the linear acenes. Isosurface representations of $\Delta\rho$ for the ^1L_a and ^1L_b excited states, computed at the TD-B3LYP level, are depicted in Figure 10. In these isosurface representations, we have chosen contour values that encapsulate 60% of the positive and negative lobes of $\Delta\rho$, a value that was selected in order to obtain plots that are qualitatively similar to those published in ref 37, where $\Delta\rho$ was computed at the level of second-order approximate coupled-cluster theory (CC2). Consistent with the CC2 difference densities plotted in ref 37, the TD-B3LYP difference densities in Figure 10 show that the $S_0 \rightarrow {}^1L_a$ excitations are associated with a greater degree of local charge reorganization, as compared to the $S_0 \rightarrow {}^1L_b$ excitations. This fact was previously noted by Wong and Hsieh,[37] as an explanation for improved performance of TD-LRC-DFT for the ^1L_a state.

Unfortunately, the picture becomes a bit more muddled if one plots isosurfaces that contain a larger fraction of $\Delta\rho$, as can be seen from the 95% isocontour surfaces, computed at the TD-B3LYP level, that are depicted on the left side of Figure 11. These isosurface plots fail to provide any clear evidence that the ^1L_a state exhibits a greater degree of charge separation than does the ^1L_b state. Difference densities obtained at the TD-B3LYP level are nearly identical to those obtained at the TD-LRC-ωPBE level, as can be seen by plotting the difference between the difference densities,

$$\Delta\Delta\rho = \Delta\rho(\text{B3LYP}) - \Delta\rho(\text{LRC-}\omega\text{PBE}) \qquad (3)$$

Isosurface representations of $\Delta\Delta\rho$ are similar for both states (see Figure 11). In other words, any sort of charge separation that one might infer on the basis of $\Delta\rho$ for one method is present also in the other method. Analysis of $\Delta\rho$ therefore cannot explain the fact that non-LRC functionals exhibit a qualitatively different size-dependence for the ^1L_a state, as compared to LRC functionals.

Figure 12 presents isosurface representations of $\Delta\rho$ and $\Delta\Delta\rho$ for two different nonlinear PAHs, **7** and **11**. For **7**, where the TD-B3LYP excitation energy for ^1L_a is reasonably accurate, we find almost no difference between $\Delta\rho$ computed at the TD-B3LYP level and $\Delta\rho$ computed at the TD-LRC-ωPBE level; in fact, differences in $\Delta\rho$ between these two functionals are much more

Table 5. Values of the CT Metric (Equation 4) for the ^1L_a State and the ^1L_b State of the Linear Acene Series, Computed at the TD-B3LYP Level

	$n = 2$	$n = 3$	$n = 4$	$n = 5$	$n = 6$
$\Lambda(^1L_a)$	0.86	0.83	0.89	0.85	0.90
$\Lambda(^1L_b)$	0.62	0.61	0.63	0.64	0.65
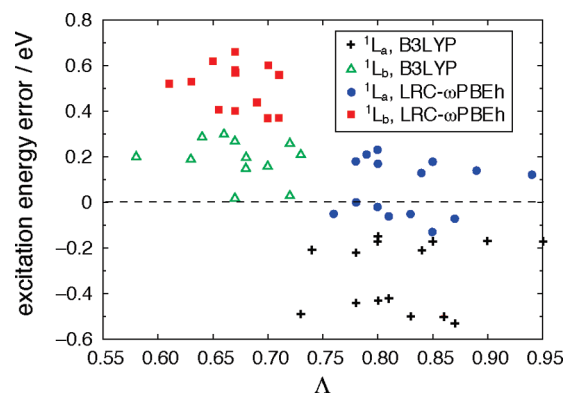
Figure 13. Errors in TD-DFT excitation energies for the nonlinear PAHs, plotted as a function of the CT metric, Λ. The LRC-ωPBE and LRC-ωPBEh functionals afford similar results, so only the latter is shown here.

significant for the ^1L_b state. In the case of **11**, for which TD-B3LYP error in the ^1L_a excitation energy is large, we do see qualitative differences in $\Delta\rho$ between these two methods. However, these differences are no more significant for the ^1L_a state than they are for the ^1L_b state. (In other words, $\Delta\Delta\rho$ is similar for both states.) Since TD-B3LYP is more accurate for the ^1L_b excitation energy of **11**, while TD-LRC-ωPBE is more accurate for the ^1L_a excitation energy, this cannot explain the origin of the TD-B3LYP errors for ^1L_a.

C. Tozer's CT Metric. Tozer and co-workers[36,47] have proposed a diagnostic test to determine whether a particular TD-DFT excited state is beset by sufficient CT contamination such that the predicted excitation energy may not be reliable. This diagnostic comes in the form of a metric, Λ, given by

$$\Lambda = \frac{\sum\limits_{ia}(X_{ia} + Y_{ia})^2 O_{ia}}{\sum\limits_{jb}(X_{jb} + Y_{jb})^2} \qquad (4)$$

which is defined such that $0 \leq \Lambda \leq 1$. The quantities X_{ia} and Y_{ia} are the TD-DFT transition amplitudes (using standard notation[68]), which determine the transition density matrix, and O_{ia} is the overlap integral between $|\phi_i(\vec{r})|$ and $|\phi_a(\vec{r})|$, where ϕ_i and ϕ_a are occupied and virtual MOs, respectively. When $\Lambda = 0$, the transition in question involves donor and acceptor orbitals with no spatial overlap, and methods such as TD-B3LYP and TD-BP86 will undoubtedly underestimate the excitation energy in such cases, probably by a large amount. On the basis of a set of benchmark tests, Tozer and co-workers suggest that TD-B3LYP excitation energies are unreliable if $\Lambda < 0.3$,[36] although they later reported an example where this metric fails to detect a problematic CT state.[69]

Values of Λ for the linear acene series have been reported in ref 37 and in the Supporting Information for ref 36, but because

these data are relevant to the discussion at hand, they are also listed in Table 5. In all cases (naphthalene through hexacene), we find that $\Lambda > 0.8$ for the $S_0 \rightarrow {}^1L_a$ excitation, whereas $\Lambda \approx 0.6$ for the $S_0 \rightarrow {}^1L_b$ excitation. As was pointed out in a previous analysis of the linear acenes,[37] these values are not only above the $\Lambda = 0.3$ threshold established in previous tests, but in fact it is the ${}^1L_b$ state that exhibits the larger value of the CT metric! Furthermore, although TD-DFT errors for the $S_0 \rightarrow {}^1L_a$ excitation energy are clearly correlated with molecular size, Λ exhibits no such size dependence. This is consistent with a transition density comprised of excitations from delocalized π MOs into delocalized π^* MOs.

For the nonlinear PAHs, Figure 13 provides a plot of the excitation energy errors versus Λ; as with the linear acenes, the ${}^1L_a$ state exhibits larger values of Λ than does ${}^1L_b$. The original proposal of Λ as a useful diagnostic was based on an observed correlation between TD-DFT errors and the value of this metric,[36] but no evidence of any such correlation is found in the PAH data. On the other hand, a clear correlation is evident in the data of ref 36 only when $\Lambda \lesssim 0.5$, whereas $\Lambda > 0.55$ for all of the PAHs. Moreover, the range of Λ values that is obtained, for a given excited state, is no different for TD-B3LYP than it is for the TD-LRC-DFT methods. This is consistent with the observed similarity between the difference densities computed using different functionals, and both observations are consistent with the notion that the calculated ${}^1L_a$ (or ${}^1L_b$) electron density is not significantly different among the various functionals. What changes from one functional to the next is the manner in which the excitation energies *depend* on this electron density.

D. Atomic Partition of Particle/Hole Densities. A potentially useful way to analyze the extent of charge separation is to decompose the transition density matrices into "particle" and "hole" components, which can then be analyzed separately. To do this, we define a density matrix $\mathbf{D}^{elec}$ for the excited electron, whose matrix elements are

$$D_{ab}^{elec} = \sum_i (\mathbf{X}^\dagger + \mathbf{Y}^\dagger)_{ai}(\mathbf{X} + \mathbf{Y})_{ib} \qquad (5)$$

A density matrix, $\mathbf{D}^{hole}$, for the hole that is left behind in the occupied space is defined similarly:

$$D_{ij}^{hole} = \sum_a (\mathbf{X} + \mathbf{Y})_{ia}(\mathbf{X}^\dagger + \mathbf{Y}^\dagger)_{aj} \qquad (6)$$

Note that $\mathbf{D}^{elec} + \mathbf{D}^{hole} = \Delta\mathbf{P}$ is the difference between the ground- and excited-state one-electron density matrices. Upon transforming $\mathbf{D}^{elec}$ and $\mathbf{D}^{hole}$ into the AO basis, one can write

$$\Delta q = \text{tr}(\mathbf{D}^{elec}\mathbf{S}) = -\text{tr}(\mathbf{D}^{hole}\mathbf{S}) \qquad (7)$$

where $\mathbf{S}$ is the AO overlap matrix. The quantity Δq is the total charge that is transferred from the occupied space to the virtual space. For TDA calculations, $\Delta q = -1$ (exactly), but deviations from -1 are possible in full TD-DFT calculations. (Typically, however, the Y_{ia} amplitudes are quite small; hence, $\Delta q \approx -1$ even in full TD-DFT calculations.)

Equation (7) immediately suggests that the matrix products $\mathbf{D}^{elec}\mathbf{S}$ and $\mathbf{D}^{hole}\mathbf{S}$ are amenable to Mulliken-style population analysis, just as $\mathbf{PS}$ is analyzed in ground-state calculations.[70] In particular, the matrix element $(\mathbf{D}^{elec}\mathbf{S})_{\nu\nu}$ represents the νth AO's contribution to the excited electron, while $(\mathbf{D}^{hole}\mathbf{S})_{\nu\nu}$ is a contribution to the hole. The sum of these quantities,

$$\Delta q_\nu = (\mathbf{D}^{elec}\mathbf{S})_{\nu\nu} + (\mathbf{D}^{hole}\mathbf{S})_{\nu\nu} \qquad (8)$$
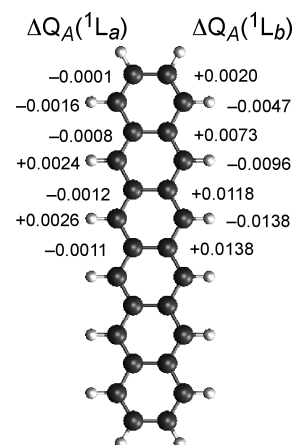
Figure 14. Differences between excited-state and ground-state Mulliken charges [ΔQ_A, from eq (9)] for the carbon atoms in hexacene, computed at the TD-B3LYP/6-31G* level. Only the symmetry-unique carbon atoms have been labeled, with $S_0 \rightarrow {}^1L_a$ charge differences on the left side and $S_0 \rightarrow {}^1L_b$ charge differences on the right side.

represents the contribution to Δq arising from the νth AO, and

$$\Delta Q_A = \sum_{\nu \in A} \Delta q_\nu \qquad (9)$$

is the change in the Mulliken population of atom A, upon electronic excitation. Generalization to Löwdin-style population analysis[70] is straightforward, and we have implemented these "particle/hole" population analyses into a locally modified version of Q-Chem. Because Mulliken and Löwdin analysis often produce erratic results in extended basis sets, we employ the somewhat more compact 6-31G* basis set for these calculations, rather than the cc-pVTZ basis that is used elsewhere in this work.

The expectation, based on valence-bond considerations, is that the ${}^1L_a$ state should exhibit charge separation on the length scale of C—C bonds. In light of this, it is surprising that both Mulliken and Löwdin population analyses afford an alternating pattern of charges on the carbon atoms *for the ${}^1L_b$ state* (see Figure 14). To some extent, the ${}^1L_a$ state exhibits a similar pattern, but in this case there is an additional (albeit quite small) accumulation of negative charge at the ends of the molecule. This suggests that a small amount of charge is pushed to extremities of the molecule in the ${}^1L_a$ state but not in the case of ${}^1L_b$. However, the magnitudes of the charge differences, ΔQ_A, are difficult to reconcile with the valence-bond interpretations of ${}^1L_a$ and ${}^1L_b$; charge differences on individual carbon atoms are ~100 times larger in the ${}^1L_b$ state than in the ${}^1L_a$ state. (This is true even when we resort to minimal basis sets, in the interest of obtaining more "chemically intuitive" Mulliken charges.) Analysis of the particle and hole contributions to ΔQ_A shows that these contributions, which must have opposite sign, are typically ~100 times larger than ΔQ_A itself. This is indicative of delocalized NTOs, with a very subtle pattern of net charge separation.

Mulliken charge differences for PAHs **7**, **10**, and **11**, computed at the TD-B3LYP/6-31G* level, are shown in Figure 15. (Charges computed using LRC functionals are quite similar.) As compared to the linear acenes, these examples exhibit far less disparity between the charge differences associated with the $S_0 \rightarrow {}^1L_a$ and $S_0 \rightarrow {}^1L_b$ excitations. The ΔQ_A values in both **7** and **11** suggest some intramolecular charge separation (from the bottom of the molecule to the top of the molecule, as it is shown

1303

dx.doi.org/10.1021/ct100607w |*J. Chem. Theory Comput.* 2011, 7, 1296–1306
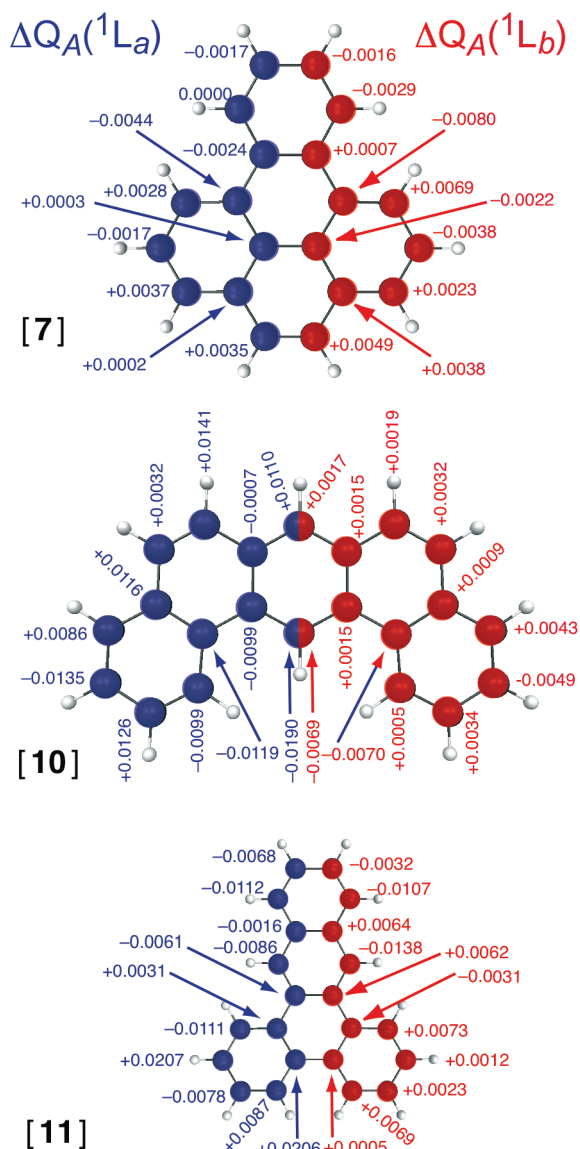
Figure 15. Differences between excited-state and ground-state Mulliken charges for the carbon atoms in PAHs **7**, **10**, and **11**. Charges were computed at the TD-B3LYP/6-31G* level and are listed for the symmetry-unique carbon only; blue labels (left side) correspond to ^1L_a and red labels (right side) correspond to ^1L_b.

in Figure 15), and this effect appears to be more significant in **11** than it is in **7**.

We consider this result in light of the two partitions of the PAH data set that were introduced in section III.B. The ^1L_a excitation energy for **11** is significantly underestimated at the TD-B3LYP level, despite the fact that this molecule falls into the peri-condensed subset that has a somewhat smaller MAE as compared to the cata-condensed subset (see Table 4). PAH **10** falls into the cata-condensed and "3+" subsets, for which the TD-B3LYP MAEs are larger than they are for the full data set, and Figure 15 shows that the magnitudes of the ΔQ_A values for the $S_0 \rightarrow \, ^1L_a$ excitation in **10** are comparable to those observed for **11**, even though the former does not exhibit the sort of overall charge separation that is observed in the latter. In both **10** and **11**, the magnitudes of the ΔQ_A values are notably larger than they are in **7**.

This analysis suggests that the magnitude of the TD-B3LYP error in the ^1L_a excitation energy is somehow related to the extent of charge reorganization upon $S_0 \rightarrow \, ^1L_a$ excitation. This is certainly not a predictive metric, however, and it is further complicated by examination of the Mulliken charge differences for the $S_0 \rightarrow \, ^1L_b$ excitations in Figure 15. In both **7** and **11**, the ΔQ_A values exhibit similar patterns for both $S_0 \rightarrow \, ^1L_a$ and $S_0 \rightarrow \, ^1L_b$ excitation; namely, the Mulliken charge differences alternate in sign across the carbon backbone. The magnitudes of the ΔQ_A values are also quite similar for both states. Thus, while it appears that Mulliken charge differences may help to explain why the ^1L_a excitation energies in certain PAHs suffer larger TD-B3LYP errors than others, these charge differences are of little help in understanding why these errors are smaller for ^1L_b than for ^1L_a.

E. Summary. In view of these observations, we are left with the following situation. The trends in TD-DFT excitations energies with respect to molecular size strongly suggest that the ^1L_a state in many different PAHs exhibits some sort of CT or charge-separation character that is not present in the ^1L_b state. The fact that TD-LRC-DFT calculations largely mitigate this problem adds to the (circumstantial) evidence for CT character in the ^1L_a state of the linear acene molecules. At the same time, attempts to discern this charge-separated character from the NTOs or transition densities are quite tenuous, and at best these analyses suggest only a very slight concentration of charge at the ends of the molecule. It is essentially impossible to discern any CT character from the MOs or difference density plots, and the TD-DFT charge-overlap metric introduced by Tozer and co-workers[36,47] also fails to raise any warning flags. Mulliken- or Löwdin-style analyses of the transition densities and excited-state atomic charges offer some insight into the nature of the charge separation, but some such charge separation is observed even in the case of excitations where TD-B3LYP predicts the excitation energy accurately.

V. CONCLUSIONS

We have evaluated the performance of TD-DFT and TD-LRC-DFT approaches for calculation of the vertical excitation energies of the ^1L_a and ^1L_b states of various PAHs. While methods such as TD-B3LYP and TD-BP86 provide reasonably accurate values for the ^1L_b excitation energies, ^1L_a excitation energies are consistently underestimated, with errors that increase as the size of the molecule increases. In contrast, TD-LRC-DFT excitation energies are accurate to within ~0.1 eV for the ^1L_a excitation energies. In the linear acene sequence, these methods also correctly predict a crossover point at which the ^1L_a state becomes lower in energy than the ^1L_b state. At the same time, ^1L_b excitation energies are systematically overestimated by LRC functionals (but without any clear size-dependent trend) and are somewhat less accurate than TD-B3LYP results.

The most important result to emerge from this work is an indication, based upon size-dependent trends in excitation energies, that the ^1L_a excited state in many PAHs exhibits some sort of charge-separated character that is not present in the ^1L_b state. This feature causes ^1L_a excitation energies to diverge from experimental values as the size of the molecule increases, when methods such as TD-B3LYP, TD-PBE0, or TD-BP86 are employed. Our hypothesis concerning the charge-separated nature of the ^1L_a state is consistent with the valence-bond language that has long been used to describe the ^1L_a and ^1L_b states, according to which the ^1L_a state is ionic while ^1L_b is

covalent.[30−35] However, although the ionic character of ^1L_a emerges cleanly from analysis of TD-PPP calculations,[28] where it correlates well with the error in TD-BP86 excitation energies, analysis of all-electron TD-DFT calculations is much more ambiguous in this respect.

While it is possible, in post hoc analysis, to rationalize the relatively ionic character of ^1L_a by examining TD-DFT transition densities and NTOs, other forms of analysis—including TD-DFT difference density plots and Mulliken population analysis of particle and hole density matrices—do not obviously suggest that ^1L_a exhibits any more CT character than does ^1L_b. A metric specifically designed to detect and quantify CT character in TD-DFT calculations,[36] and which has been successful in this respect, for a variety of molecules,[36,47] also fails to indicate that ^1L_a is more "CT-like" than ^1L_b. This metric is certainly not perfect, and Peach et al.[69] have identified a case where it fails to flag an excitation that (based on examination of the MOs) is clearly a CT state and where the excitation energy is substantially under-estimated at the TD-PBE and TD-PBE0 levels. The difference here is that the ^1L_a states in the PAHs are *not* clear examples of CT states.

These observations suggest the possibility that medium- to large-size conjugated organic molecules may exhibit subtle charge-separation effects that are difficult to identify a priori but which cause conventional TD-DFT methods to overstabilize these states, possibly by a significant amount. This is a potentially serious problem in cases where TD-DFT is applied to molecules that are too large to perform any high-level ab initio benchmarks and where reliable experimental data are unavailable. Further analysis is required in order to develop a diagnostic that can automatically detect such states. In the meantime, we recommend performing TD-DFT calculations with both LRC functionals (e.g., LRC-ωPBE or LRC-ωPBEh) and also non-LRC functionals (e.g., B3LYP or PBE0) so that the results may be compared and potentially problematic states may be detected.

■ ASSOCIATED CONTENT

Ⓢ Supporting Information. Cartesian coordinates for the optimized PAH geometries, TD-DFT excitation energies, and values of the Λ metric. This information is available free of charge via the Internet at http://pubs.acs.org.

■ AUTHOR INFORMATION

Corresponding Author
*E-mail: herbert@chemistry.ohio-state.edu.

■ ACKNOWLEDGMENT

■ REFERENCES

(1) Dreuw, A.; Weisman, J. L.; Head-Gordon, M. *J. Chem. Phys.* **2003**, *119*, 2943–2946.

(2) Dreuw, A.; Head-Gordon, M. *J. Am. Chem. Soc.* **2004**, *126*, 4007–4016.

(3) Magyar, R. J.; Tretiak, S. *J. Chem. Theory Comput.* **2007**, *3*, 976–987.

(4) Lange, A. W.; Herbert, J. M. *J. Am. Chem. Soc.* **2009**, *131*, 3913–3922.

(5) Bernasconi, L.; Sprik, M.; Hutter, J. *J. Chem. Phys.* **2003**, *119*, 12417–12431.

(6) Neugebauer, J.; Louwerse, M. J.; Baerends, E. J.; Wesołowski, T. A. *J. Chem. Phys.* **2005**, *122*, 094115-1–094115-13.

(7) Lange, A.; Herbert, J. M. *J. Chem. Theory Comput.* **2007**, *3*, 1680–1690.

(8) Iikura, H.; Tsuneda, T.; Yanai, T.; Hirao, K. *J. Chem. Phys.* **2001**, *115*, 3540–3544.

(9) Tawada, Y.; Tsuneda, T.; Yanagisawa, S.; Yanai, T.; Hirao, K. *J. Chem. Phys.* **2004**, *120*, 8425–8433.

(10) Song, J.-W.; Hirosawa, T.; Tsuneda, T.; Hirao, K. *J. Chem. Phys.* **2007**, *126*, 154105-1–154105-7.

(11) Sato, T.; Tsuneda, T.; Hirao, K. *J. Chem. Phys.* **2007**, *126*, 234114-1–234114-12.

(12) Yanai, T.; Tew, D. P.; Handy, N. C. *Chem. Phys. Lett.* **2004**, *393*, 51–57.

(13) Peach, M. J. G.; Cohen, A. J.; Tozer, D. J. *Phys. Chem. Chem. Phys.* **2006**, *8*, 4543–4549.

(14) Vydrov, O. A.; Scuseria, G. E. *J. Chem. Phys.* **2006**, *125*, 234109-1–234109-9.

(15) Henderson, T. M.; Janesko, B. G.; Scuseria, G. E. *J. Chem. Phys.* **2008**, *128*, 194105-1–194105-9.

(16) Henderson, T. M.; Janesko, B. G.; Scuseria, G. E. *J. Phys. Chem. A* **2008**, *112*, 12530–12542.

(17) Chai, J.-D.; Head-Gordon, M. *J. Chem. Phys.* **2008**, *128*, 084106-1–084106-15.

(18) Rohrdanz, M. A.; Herbert, J. M. *J. Chem. Phys.* **2008**, *129*, 034107-1–034107-9.

(19) Rohrdanz, M. A.; Martins, K. M.; Herbert, J. M. *J. Chem. Phys.* **2009**, *130*, 054112-1–054112-8.

(20) Baer, R.; Livshits, E.; Salzner, U. *Annu. Rev. Phys. Chem.* **2010**, *61*, 85–109.

(21) Savin, A. In *Recent Advances in Density Functional Methods*, Part I; *Recent Advances in Computational Chemistry*, Vol. 1; Chong, D. P., Ed.; World Scientific: Singapore, 1995; pp 129−153.

(22) Gill, P. M. W.; Adamson, R. D.; Pople, J. A. *Mol. Phys.* **1996**, *88*, 1005–1009.

(23) Adamson, R. D.; Dombroski, J. P.; Gill, P. M. W. *J. Comput. Chem.* **1999**, *20*, 921–927.

(24) Tozer, D. J.; Amos, R. D.; Handy, N. C.; Roos, B. O.; Serrano-Andrés, L. *Mol. Phys.* **1999**, *97*, 859–868.

(25) Silva-Junior, M. R.; Schreiber, M.; Sauer, S. P. A.; Thiel, W. *J. Chem. Phys.* **2008**, *129*, 104103-1–104103-14.

(26) Jacquemin, D.; Wathelet, V.; Perpéte, E. A.; Adamo, C. *J. Chem. Theory Comput.* **2009**, *5*, 2420–2435.

(27) Grimme, S.; Parac, M. *ChemPhysChem* **2003**, *4*, 292–295.

(28) Parac, M.; Grimme, S. *Chem. Phys.* **2003**, *292*, 11–21.

(29) Platt, J. R. *J. Chem. Phys.* **1949**, *17*, 484–495.

(30) Handa, T. *Bull. Chem. Soc. Jpn.* **1963**, *36*, 235–247.

(31) Orchin, M.; Jaffé, H. H. *Symmetry. Orbitals, and Spectra*; Wiley: New York, 1971.

(32) Malloci, G.; Mulas, G.; Cappellini, G.; Joblin, C. *Chem. Phys.* **2007**, *340*, 43–58.

(33) Hashimoto, T.; Nakano, H.; Hirao, K. *J. Chem. Phys.* **1996**, *104*, 6244–6258.

(34) Hirao, K.; Nakano, H.; Nakayama, K.; Dupuis, M. *J. Chem. Phys.* **1996**, *105*, 9227–9239.

(35) Hirao, K.; Nakano, H.; Nakayama, K. *J. Chem. Phys.* **1997**, *107*, 9966–9974.

(36) Peach, M. J. G.; Benfield, P.; Helgaker, T.; Tozer, D. J. *J. Chem. Phys.* **2008**, *128*, 044118-1–044118-8.

(37) Wong, B. M.; Hsieh, T. H. *J. Chem. Theory Comput.* **2010**, *6*, 3704–3712.

(38) Zilberg, S.; Haas, Y.; Shaik, S. *J. Phys. Chem.* **1995**, *99*, 16558–16565.

(39) Gill, P. M. W.; Johnson, B. G.; Pople, J. A. *Chem. Phys. Lett.* **1993**, *209*, 506–512.

(40) Hirata, S.; Head-Gordon, M. *Chem. Phys. Lett.* **1999**, *314*, 291–299.

(41) Shao, Y.; Fusti-Molnar, L.; Jung, Y.; Kussmann, J.; Ochsenfeld, C.; Brown, S. T.; Gilbert, A. T. B.; Slipchenko, L. V.; Levchenko, S. V.; O'Neill, D. P., Jr.; R, A. D.; Lochan, R. C.; Wang, T.; Beran, G. J. O.; Besley, N. A.; Herbert, J. M.; Lin, C. Y.; Van Voorhis, T.; Chien, S. H.; Sodt, A.; Steele, R. P.; Rassolov, V. A.; Maslen, P. E.; Korambath, P. P.; Adamson, R. D.; Austin, B.; Baker, J.; Byrd, E. F. C.; Dachsel, H.; Doerksen, R. J.; Dreuw, A.; Dunietz, B. D.; Dutoi, A. D.; Furlani, T. R.; Gwaltney, S. R.; Heyden, A.; Hirata, A.; Hsu, C.-P.; Kedziora, G.; Khalliulin, R. Z.; Klunzinger, P.; Lee, A. M.; Lee, M. S.; Liang, W.; Lotan, I.; Nair, N.; Peters, B.; Proynov, E. I.; Pieniazek, P. A.; Rhee, Y. M.; Ritchie, J.; Rosta, E.; Sherrill, C. D.; Simmonett, A. C.; Subotnik, J. E.; Woodcock, H. L., III; Zhang, W.; Bell, A. T.; Chakraborty, A. K.; Chipman, D. M.; Keil, F. J.; Warshel, A.; Hehre, W. J.; Schaefer, H. F., III; Kong, J.; Krylov, A. I.; Gill, P. M. W.; Head-Gordon, M. *Phys. Chem. Chem. Phys.* **2006**, *8*, 3172–3191.

(42) Becke, A. D. *Phys. Rev. A* **1988**, *38*, 3098–3100.

(43) Lee, C.; Yang, W.; Parr, R. G. *Phys. Rev. B* **1988**, *37*, 785–789.

(44) Tsuneda, T.; Suzumura, T.; Hirao, K. *J. Chem. Phys.* **1999**, *110*, 10664–10678.

(45) Perdew, J. P.; Burke, K.; Ernzerhof, M. *Phys. Rev. Lett.* **1996**, *77*, 3865–3868.

(46) We use "μ" to indicate LRC functionals in which the short-range GGA exchange functional is constructed according to the procedure of Iikura et al.[8] Short-range versions of Becke's B88 exchange functional[42] ("μB88") and Perdew–Burke–Ernzerhof exchange[45] ("μPBE") are available in Q-Chem. Henderson et al.[15] have developed an alternative version of short-range PBE exchange that they call ωPBE, and we adopt the same notation. The notation "LC-BOP" has also been used for the functional that we call LRC-μBOP,[10] and "LC-ωPBE" has been used for what we call LRC-ωPBE,[15,26] albeit with different parameters than those used here. The LRC-ωPBE functional has has also been called simply "ωPBE",[47] but we dislike this particular nomenclature, because ωPBE exchange is sometimes used *without* long-range HF exchange.[48]

(47) Plötner, J.; Tozer, D. J.; Dreuw, A. *J. Chem. Theory Comput.* **2010**, *6*, 2315–2324.

(48) Heyd, J.; Scuseria, G. E. *J. Chem. Phys.* **2004**, *121*, 1187–1192.

(49) Lange, A. W.; Rohrdanz, M. A.; Herbert, J. M. *J. Phys. Chem. B* **2008**, *112*, 6304–6308.

(50) Wong, B. M.; Cordaro, J. G. *J. Chem. Phys.* **2008**, *129*, 214703-1–214703-8.

(51) Wong, B. M.; Piacenza, M.; Della Sala, F. *Phys. Chem. Chem. Phys.* **2009**, *11*, 4498–4508.

(52) Wang, Y.-L.; Wu, G.-S. *Int. J. Quantum Chem.* **2007**, *108*, 430–439.

(53) Stein, T.; Kronik, L.; Baer, R. *J. Chem. Phys.* **2009**, *131*, 244119-1–244119-5.

(54) Scher, H.; Montroll, E. W. *Phys. Rev. B* **1975**, *12*, 2455–2477.

(55) Callis, P. R. *Int. J. Quantum Chem.* **1984**, *26*, 579–588.

(56) Rogers, D. M.; Besley, N. A.; O'Shea, P.; Hirst, J. D. *J. Phys. Chem. B* **2005**, *109*, 23061–23069.

(57) Clar, E. *Polycyclic Hydrocarbons*, Vol. 1; Academic Press: London, 1964.

(58) Vijayalakshmi, K. P.; Suresh, C. H. *New J. Chem.* **2010**, *34*, 2132–2138.

(59) Birks, J. B. *Photophysics of Aromatic Molecules*; Wiley: New York, 1970.

(60) Schmidt, W. *J. Chem. Phys.* **1977**, *66*, 828–845.

(61) Champagne, B.; Perpète, E. A.; van Gisbergen, S. J. A.; Baerends, E.-J.; Snijders, J. G.; Soubra-Ghaoui, C.; Robins, K. A.; Kirtman, B. *J. Chem. Phys.* **1998**, *109*, 10489–10498.

(62) Champagne, B.; Perpète, E. A.; Jacquemin, D.; van Gisbergen, S. J. A.; Baerends, E.-J.; Soubra-Ghaoui, C.; Robins, K. A.; Kirtman, B. *J. Phys. Chem. A* **2000**, *104*, 4755–4763.

(63) Sekino, H.; Maeda, Y.; Kamiya, M.; Hirao, K. *J. Chem. Phys.* **2007**, *126*, 014107-1–014107-6.

(64) Pariser, R.; Parr, R. G. *J. Chem. Phys.* **1953**, *21*, 466–471.

(65) Pariser, R.; Parr, R. G. *J. Chem. Phys.* **1953**, *21*, 767–776.

(66) Pople, J. A. *Trans. Faraday Soc.* **1953**, *49*, 1375–1385.

(67) Martin, R. L. *J. Chem. Phys.* **2003**, *118*, 4775–4777.

(68) Dreuw, A.; Head-Gordon, M. *Chem. Rev.* **2005**, *105*, 4009–4037.

(69) Peach, M. J. G.; Le Sueur, C. R.; Ruud, K.; Guillaume, M.; Tozer, D. J. *Phys. Chem. Chem. Phys.* **2009**, *11*, 4465–4470.

(70) Szabo, A.; Ostlund, N. S. *Modern Quantum Chemistry*; Collier Macmillan: London, 1982.

(71) Haranczyk, M.; Gutowski, M. *J. Chem. Theory Comput.* **2008**, *4*, 689–693.

(72) Humphrey, W.; Dalke, A.; Schulten, K. *J. Mol. Graphics* **1996**, *14*, 33–38.

(73) Bode, B. M.; Gordon, M. S. *J. Mol. Graphics Modell.* **1998**, *16*, 133–138.